

Article

PVC Detection through a Hybrid SEIRA Substrate and Refractive Index Sensor Based on Metamaterial Perfect Absorbers

Chieh-Ting Lin ¹, Ta-Jen Yen ^{1,2} and Tsung-Yu Huang ^{3,*}

¹ Department of Materials Science and Engineering, National Tsing Hua University, Hsinchu 300044, Taiwan; rdg01101@gmail.com (C.-T.L.); tjyen@mx.nthu.edu.tw (T.-J.Y.)

² Department of Materials Science Center for Nanotechnology, Materials Science, and Microsystems, National Tsing Hua University, Hsinchu 300044, Taiwan

³ Department of Materials Engineering, Ming Chi University of Technology, New Taipei City 243303, Taiwan

* Correspondence: huang.tsungyu@mail.mcut.edu.tw

Abstract: Simultaneous surface enhanced infrared absorption (SEIRA) with Fano resonance and refractive index (RI) sensing are proposed via a split-ring-resonator-based metamaterial perfect absorber (MPA) to detect polyvinyl chloride (PVC), a commonly used polymer but one that was recently prohibited in many areas such as Europe. This bifunctional sensor could provide a label-free and qualitative PVC detection through SEIRA coupled to the vibration mode and a quantitative measurement through RI sensing. To design the MPA, the main operating frequency is targeted at 615 cm^{-1} for C-Cl bond of PVC. Transition from a reflectance dip to a peak, i.e., Fano resonance was observed at y polarization in both simulation and experiments, evidencing the existence of PVC. On the other hand, to test the RI sensing ability of the MPA, different RI (from 1 to 1.5) of analytes and different thicknesses (from 109 to 1050 nm) of polymethyl methacrylate (PMMA) were applied to the MPA in simulation and experiments, respectively. The simulated sensitivities are 4045 and 2361 nm/RIU for the first and third modes of the MPA, respectively, while the measured sensitivities based on PMMA are 3713 and 1694 nm/RIU. Overall, the detection limit of PVC could be down to 0.5% in experiments, which outweighs the current measurement limit of 10% through infrared absorption measurement.

Keywords: SEIRA; Fano resonance; metamaterial perfect absorber; chemical detection



Citation: Lin, C.-T.; Yen, T.-J.; Huang, T.-Y. PVC Detection through a Hybrid SEIRA Substrate and Refractive Index Sensor Based on Metamaterial Perfect Absorbers. *Coatings* **2021**, *11*, 789.

<https://doi.org/10.3390/coatings11070789>

Academic Editor: Anna Palau

Received: 7 May 2021

Accepted: 18 June 2021

Published: 30 June 2021

Publisher's Note: MDPI stays neutral with regard to jurisdictional claims in published maps and institutional affiliations.



Copyright: © 2021 by the authors. Licensee MDPI, Basel, Switzerland. This article is an open access article distributed under the terms and conditions of the Creative Commons Attribution (CC BY) license (<https://creativecommons.org/licenses/by/4.0/>).

1. Introduction

To date, infrared (IR) absorption spectroscopy has been sophisticated and well-developed technique that is widely employed for the detection of functional groups, i.e., a molecule's "finger print". Consequently, the IR absorption spectroscopy could provide characterization of analytes' structures, compositions, and even orientations. However, the weak intensity of a molecule's IR absorption signal not only degrades the sensitivity of the sensor but also reduces possible applications of single-molecular detection. In order to enhance sensitivity, surface-enhanced infrared absorption (SEIRA) [1–3] has been widely used for decades. The key point to SEIRA is the so-called electromagnetic 'hot spots', where the electromagnetic field is concentrated. Furthermore, by tuning the corresponding plasmonic resonant frequency to overlap with vibrational bands of targeted analytes, an additional enhancement of SEIRA is expected because of the coupling between the plasmonic and vibrational modes, i.e., leading to the presence of Fano-resonance [4–6]. In general, SEIRA with Fano resonance provided a label-free molecular detection with higher sensitivity. Still, such a technique possessed some insufficiencies such as sensitiveness to the analytes' distributions and nonlinear responses to the analytes' concentrations [7]. On the other hand, it is well-known that an increase of the refraction index (RI) surrounding plasmonic structures would induce red-shifts of their resonance frequency. Such shifts

are typically linear to the RI changes, hence promising quantitative detection of analytes. Furthermore, the sensitivity of RI sensing could also be boosted by hot spots of plasmonic structures [8]. Nowadays, RI sensing of plasmonic structures is being found in many different research fields such as bio-sensing [9–11], bio-imaging [12,13] and chemical detection [14,15]. Yet, the main drawback of the RI sensing is its non-specific detection, thus hindering its practical applications in many fields. Finally, polyvinyl chloride (PVC) is a commonly used polymer in many different commercial products such as children's toys, shoes, and packing materials [16,17]. However, due to the emergence of environmental awareness and protection, PVC was restricted in many different countries or areas, for example, Europe, Sweden, and New York. Unfortunately, PVC detection is burdensome and not accurate enough, since only PVC with a concentration as high as 10% could be distinguished by conventional infrared absorption measurement.

As previously mentioned, there appear to be many different plasmonic structures such as nanoscale particles/metallic islands [18,19] or metamaterials [20–22] used to create hot spots, achieving SEIRA and RI sensing with higher sensitivity. Among so many different plasmonic structures and metamaterials, metamaterial perfect absorber (MPA) is the most promising candidate, since MPAs possess stronger 'hot spots' [23–26] and stable performances compared to a nanoparticle-based sensor. Various types of MPAs were proposed, for example, an MPA constructed by vertical side walls for gas sensing [27], an MPA integrated with microfluidic channels [28], etc. Still, since our target is PVC that is easy to agglomerate, the inhomogeneous distribution of PVC would cause much fluctuation of the detected signals and the blocking of sensing channels. Also, there appear to be few discussions about SEIRA with Fano resonance and RI sensing in a single sensor [29], which further motivated us to conduct an integration of SEIRA substrates and RI sensors into a single device. To address the abovementioned issues, we proposed a split-ring-resonator-based metamaterial perfect absorber (MPA) with multiple resonance peaks that could provide SEIRA with Fano resonance and RI sensing, simultaneously, for PVC detection. Note that SEIRA with Fano resonance is an indicator for the existence of PVC, while RI sensing could provide quantitative detection with respect to the concentration of PVC.

2. Materials and Methods

To excite Fano resonance, it is very important to match functional groups of PVC to the resonance frequency of the MPA. It is worth mentioning that once we applied PVC on the MPA, the corresponding resonance frequency would red shift; thus, we needed to take this issue into consideration and design a higher operating frequency of the MPA within free space. In contrast, each resonance mode could conduct RI sensing with a shift of resonance frequency. Therefore, in the design, to decide the target resonance frequency of the MPA for PVC detection became our first priority. For PVC, there appear to be a few different representative vibrational modes, for example, C-H stretching mode at 2890–2958 cm^{-1} , and C-Cl bond at 616–690 cm^{-1} [17]. In this work, we used the C-Cl bond at 616–690 cm^{-1} as an indicator for PVC because the C-Cl bond is more unique compared to the C-H modes that are common in other organic materials. In simulation, we employed the finite integration method to simulate our proposed MPA. The MPA was composed of three layers including an upper split-ring resonator array, a dielectric spacer, and a continuous ground plane. It is worth mentioning that the SRR was chosen because SRRs were the first proposed metamaterial and have been intensively investigated, which shortened our design procedure of the MPA. The metal and dielectric used here were gold and silica, respectively, due to their relatively low losses and inert chemical properties. The corresponding top view and side view of the MPA are depicted in Figure 1a. Here, L is 6.5 μm , g = 1.65 μm , w = 5.5 μm , w_1 = 1.1 μm , t = 0.5 μm , and t_m = 50 nm. Note that all the dimensional parameters of the proposed MPA were optimized based on criteria that the MPA should provide multiple resonance wavelengths where one of them matches the C-Cl absorption band and also shows stronger reflectance dips. Figure 1b,c show the reflectance spectra of the MPA for x- (perpendicular to the gap) and y- (parallel to the gap) polarization,

respectively. Here, a reflectance dip was observed at 652 cm^{-1} for y-polarization while there was no resonance behavior at the same wavenumber for x-polarization. Furthermore, there were multiple resonance modes at both x and y-polarization that could be applied to RI sensing.

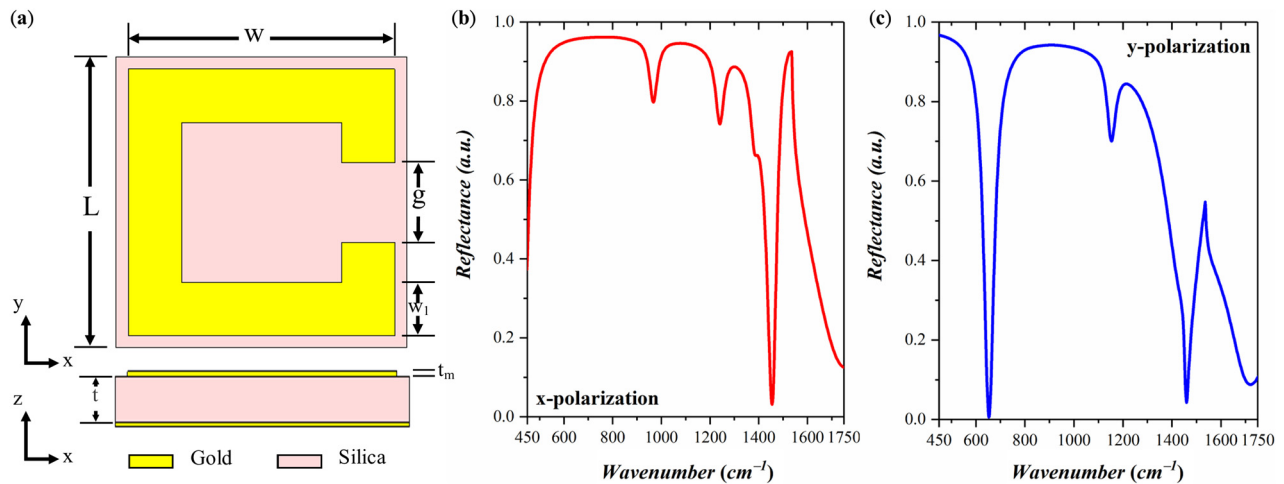


Figure 1. (a) Scheme of a split-ring-based metamaterial perfect absorber (MPA). Here, L is $6.5\ \mu\text{m}$, $g = 1.65\ \mu\text{m}$, $w = 5.5\ \mu\text{m}$, $w_1 = 1.1\ \mu\text{m}$, $t = 0.5\ \mu\text{m}$, and $t_m = 50\ \text{nm}$. Reflectance spectra of the MPA for (b) x- and (c) y-polarization, respectively. A reflectance dip was observed at 652 cm^{-1} for y-polarization while no resonance behavior was found for x-polarization. Meanwhile multiple resonance dips were found for both polarizations that could serve as the target responses for refractive index (RI) sensing.

To simulate Fano resonance, we added PVC as analytes and the permittivity of PVC with its absorption band from the C-Cl bond was modeled as a Lorentz oscillator with a functional form of [30,31]

$$\varepsilon_{PVC} = \varepsilon_b + \frac{f_m \omega_0^2}{\omega_0^2 - \omega^2 - i\gamma\omega} \quad (1)$$

where ε_b is the background relative permittivity, f_m is the reduced oscillator strength, ω_0 is the C-Cl vibrational frequency, and γ is the damping frequency. Here, values for ε_b , f_m , ω_0 and γ were equal to 3, 0.04, $2\pi \times 18.5\ \text{THz}$ and 0.1 THz, respectively. After applying the Lorentz model for the C-Cl bond in PVC, the original absorption peak (i.e., the reflectance dip) of the MPA would couple to the absorption band of the C-Cl bond and become an absorption dip (i.e., reflectance peak) with two turning points as shown in Figure 2a, indicating the occurrence of Fano-resonance ($q = 0$ [32]) and the existence of the specific molecules, thus facilitating specific chemical detection. Note that for x-polarization, we could only observe a reflectance dip instead of a peak. Such a contrast further corroborates the excitation of the Fano resonance. Then, to test the sensitivity of our proposed MPA, we examined the first and third modes under different RI changes from $n = 1.0$ to $n = 1.5$ for y-polarization. From Figure 2b, the reflectance dips red-shifted accordingly and Figure 2c summarizes the resonance frequency change with respect to RI change. The corresponding sensitivities after curve fitting are 4045 and 2361 nm/RIU for the first and the third mode, respectively.

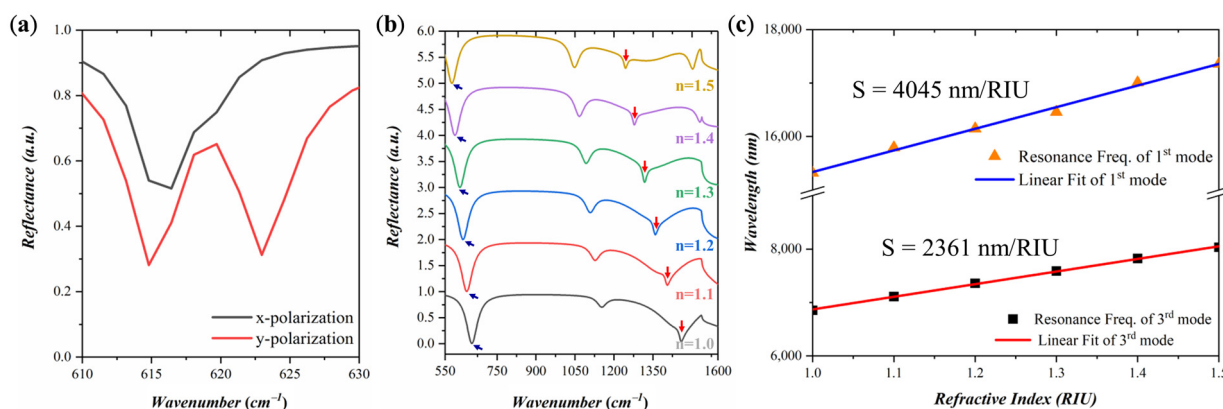


Figure 2. (a) Simulated reflectance spectrum of the proposed MPA with PVC under two different polarizations. For y polarization, the original reflectance dip was turned into a reflectance peak with two turning points. Meanwhile, there was only a reflectance dip for x-polarization. Such a contrast could corroborate the excitation of Fano-resonance, i.e., the coupling between the plasmonic modes of the MPA and the vibrational mode of PVC. (b) Simulated reflectance spectrum under different RI from $n = 1.0$ to $n = 1.5$. Here, blue and red arrows indicate different resonance wavenumbers of the first and the third modes, respectively, under different refractive indices. (c) Resonance wavelengths of the MPA with respect to the refractive index. Sensitivities in simulation were 4045 and 2361 nm/RIU, respectively.

3. Results

To fabricate the MPA, we conducted e-gun deposition for gold and silica thin films on a silicon wafer and e-beam lithography processes and e-gun deposition for the patterned upper metallic structure. Then, we measured the as-fabricated sample through μ -Fourier transformed infrared absorption (Bruker Hyperion 1000, Billerica, MA, USA) with a resolution of 4 cm^{-1} . The measured spectra for both x- and y-polarization are shown in Figure 3a,b, respectively. Note that the simulated spectra (grey dotted line) are also shown in the figure for comparison. The two agreed well with each other, especially for the targeted frequency of 636 cm^{-1} with a small deviation compared to the simulated 652 cm^{-1} . Other resonance frequencies also deviated from the simulated ones, which might have originated from different dielectric constant dispersion while the magnitude difference of the dips could be from different losses from the materials in simulation and in measurement, respectively. It is worth mentioning that the reflectance dip at around 1000 cm^{-1} should be from the absorption of silica.

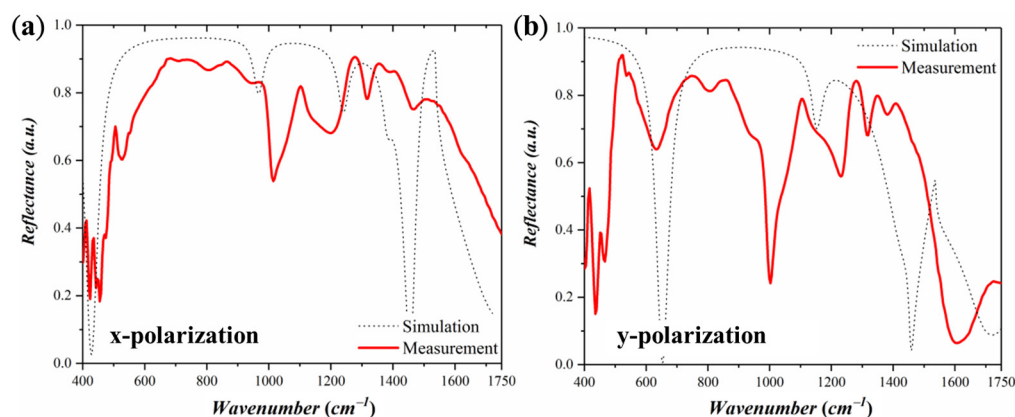


Figure 3. Measured reflectance spectra for (a) x- and (b) y-polarization. The simulated spectra are also included (gray dotted lines). The two agreed well with each other.

Next, to examine the sensitivities of the proposed MPA for RI sensing, we spin-coated polymethyl methacrylate (PMMA) on the sample with different spin rates, thus

resulting in different thicknesses of PMMA and different effective refractive index rates. The corresponding RI of PMMA and air composite materials could be predicted by the effective medium theory [33]

$$\varepsilon_{\text{eff}} = \sum_n \varepsilon_n \frac{h_n}{h_t} \quad (2)$$

where ε_{eff} is the effective permittivity of PMMA/air composite materials, ε_n and h_n are the dielectric constant and thickness of the components, and h_t is the saturation thickness of PMMA where the resonance frequency stops shifting. Here, permittivity of PMMA and air is 2.6 and 1, respectively and the saturation thickness of PMMA for the first and third modes is 515 and 660 nm, respectively. From the effective medium theory, permittivity of the complex medium composed of different fractions of PMMA and air was obtained. It is worth mentioning that neither PMMA nor air are magnetic elements, so the effective refractive index of corresponding complex medium could be derived by computing the square root of the permittivity. From Figure 4a, we could observe that the resonance wavenumbers shift with respect to different thicknesses of the applied PMMA, while the blue and red arrows indicate the resonance wavenumbers of the 1st and 3rd modes of the proposed MPA. Note that the sensitivity for the 1st and 3rd modes in experiments was 3717 and 1694 nm/RIU as depicted in Figure 4b, which were both smaller than the simulated ones stemming from the losses of PMMA in measurement.

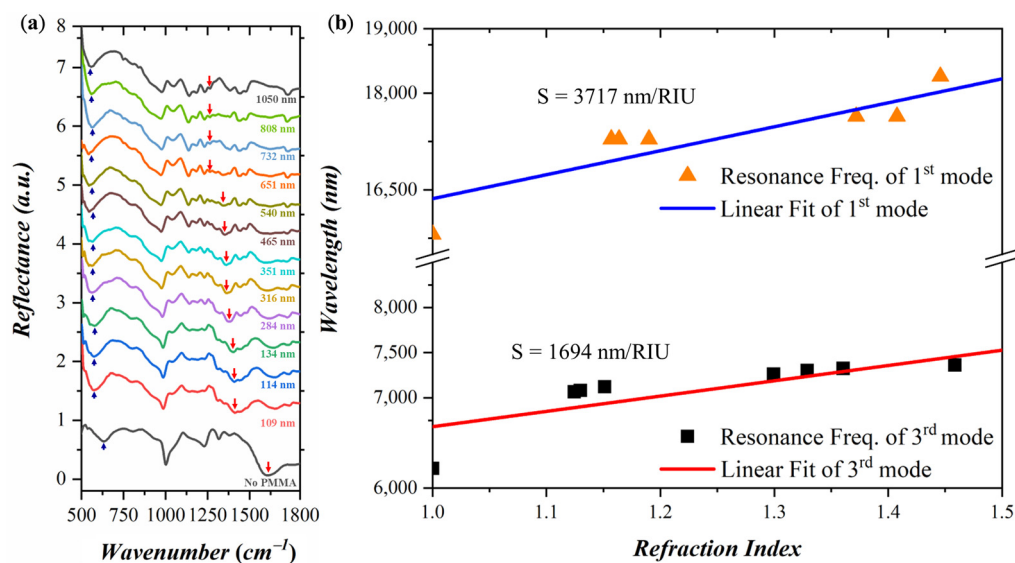


Figure 4. (a) Measured reflectance spectra with respect to different PMMA thicknesses. Shifts of the resonance frequency for the 1st and 3rd modes are labeled by blue and red arrows, respectively. (b) Variation of the resonance wavelength with respect to the refractive index. Sensitivity of the 1st and 3rd modes was 3717 and 1694, respectively.

After characterizing our MPA's SEIRA behavior with Fano resonance in simulation and RI sensitivities in both simulation and experiments, then, we applied the characterized MPA to detect PVC. First of all, according to a certification company, a 100% PVC concentration was defined as 2 g of PVC dissolved into 80 g of tetrahydrofuran (THF) for their IR sensing standard. Under this condition, we applied 0%, 0.5%, 1%, 3%, 5%, 7%, and 10% of PVC on our MPA and measured their reflectance. As shown in Figure 5, we did observe that the transition from a reflectance dip to a peak after PVC was applied on the sample. Note that in x-polarization, we could only identify a dip from PVC absorption band only, further evidencing the excitation of Fano resonance in y-polarization. To obtain the trend of responses of Fano resonance to the PVC concentration, we recorded the strongest Fano resonance at each concentration and Figure 5b depicts the responses (i.e., $\Delta R/R_0$) with respect to the PVC concentrations. The curve could be fitted to an exponential decay curve

started to saturate at around 10%. Such nonlinear responses would hinder its practical applications in molecular detection. Therefore, we also monitored the corresponding frequency shifts with different concentrations of PVC, as shown in Figure 6. The fitted curve shows a linear response, thus promising a quantitative detection. From Figure 6, we believe that the peak at around 615 cm^{-1} provided qualitative information regarding the existence of PVC while the dip within $1500\text{ to }1700\text{ cm}^{-1}$ provided linearly quantitative measurements of PVC concentrations.

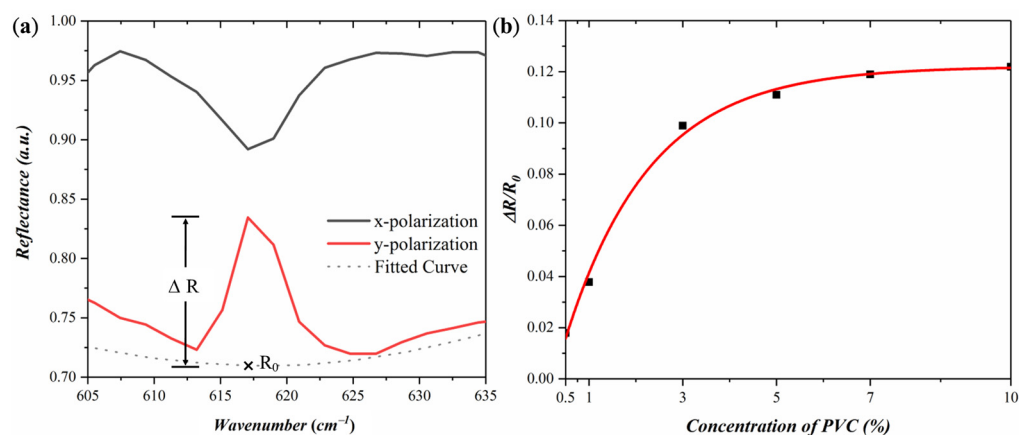


Figure 5. (a) Measured reflectance spectra with respect to two incident polarizations. To calculate the response from Fano resonance, a fitted curve with a Lorentz distribution of $y = y_0 + \frac{2A}{\pi} \frac{w}{4(x-x_c)^2 + w^2}$ was included to indicate ΔR and R_0 , the difference between the reflectance peak and dip, and the resonance frequency of the MPA without PMMA, respectively. The existence of Fano resonance corroborates the existence of PVC. (b) Plot of $\Delta R/R_0$ with respect to concentration of PMMA. $\Delta R/R_0$ became saturated at a concentration of 10% and the response was nonlinear.

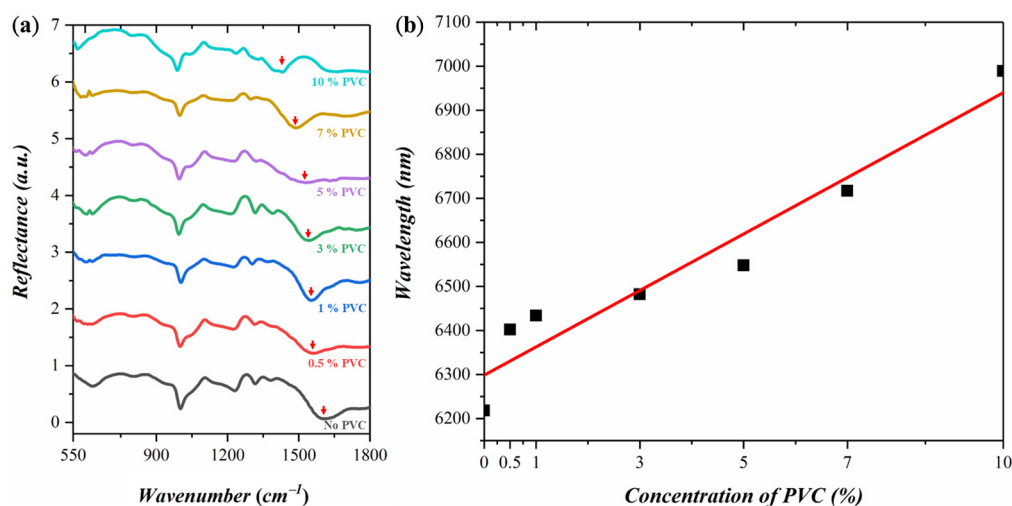


Figure 6. (a) Measured reflectance spectra with respect to different concentrations of PVC from 0% to 10%. (b) Resonance wavelengths with respect to PVC concentrations.

4. Conclusions

In this work, we present a metamaterial-based bifunctional sensor in pursuit of SEIRA detection with Fano resonance as well as RI sensing. We provide simulation and experimental verification of our MPA for both functions. Firstly, we determined the dimensions of our split ring resonator to locate the operating frequency at around 615 cm^{-1} with all the other modes for RI sensing. In simulation, the transition from a reflectance dip to a peak was observed with a PVC layer as a Lorentz oscillator. In addition, the RI sensitivities of the first and third modes for y-polarization were found to be 4045 and

2361 nm/RIU, respectively. In experiments, PMMA was employed to test the RI sensing ability of our proposed MPA. Sensitivities of 3713 and 1694 nm/RIU were obtained with different thicknesses of PMMA and with equivalent RI predicted by effective medium theory. Finally, to detect PVC, we applied different concentrations of PVC on the sample. We did observe the transition from a reflectance dip to a peak in μ -FTIR measurement. Yet, the responses (i.e., $\Delta R/R_0$) with respect to PVC concentrations were nonlinear, thus hindering its practical application. Then, we also examined the resonance wavelengths with respect to PVC concentration changes to quantify PVC concentrations with the measured resonance wavelength. Here, we could claim that we are able to distinguish PVC with a concentration as low as 0.5%. Such a bifunctional sensor would pave a route to future single molecule detection and bio-sensing and imaging.

Author Contributions: Conceptualization, T.-Y.H. and T.-J.Y.; methodology, C.-T.L. and T.-Y.H.; software, C.-T.L. and T.-Y.H.; validation, C.-T.L. and T.-Y.H.; formal analysis, C.-T.L.; investigation, C.-T.L. and T.-Y.H.; resources, T.-J.Y. and T.-Y.H.; data curation, C.-T.L., T.-J.Y. and T.-Y.H.; writing—original draft preparation, C.-T.L. and T.-Y.H.; writing—review and editing, T.-Y.H.; visualization, T.-Y.H.; supervision, T.-J.Y. and T.-Y.H.; project administration, T.-J.Y. and T.-Y.H.; funding acquisition, T.-J.Y. and T.-Y.H. All authors have read and agreed to the published version of the manuscript.

Funding: This work was supported by the Ministry of Science and Technology (MOST 104-2221-E-007-040-MY3, 107-2221-E-007-016-MY3, 106-2221-E-007-038-MY3 and 107-2218-E-131-005-MY3) and by the “High Entropy Materials Center” from The Featured Areas Research Center Program within the framework of the Higher Education Sprout Project developed by the Ministry of Education (MOE) in Taiwan (108QR001J4).

Institutional Review Board Statement: Not applicable.

Informed Consent Statement: Not applicable.

Conflicts of Interest: The authors declare no competing interests.

References

1. Aroca, R.F.; Ross, D.J.; Domingo, C. Surface-Enhanced Infrared Spectroscopy. *Appl. Spectrosc.* **2004**, *58*, 324A–338A. [[CrossRef](#)]
2. Enders, D.; Pucci, A. Surface enhanced infrared absorption of octadecanethiol on wet-chemically prepared Au nanoparticle films. *Appl. Phys. Lett.* **2006**, *88*, 184104. [[CrossRef](#)]
3. Wang, H.; Kundu, J.; Halas, N.J. Plasmonic Nanoshell Arrays Combine Surface-Enhanced Vibrational Spectroscopies on a Single Substrate. *Angew. Chem. Int. Ed.* **2007**, *46*, 9040–9044. [[CrossRef](#)] [[PubMed](#)]
4. Neubrech, F.; Pucci, A.; Cornelius, T.W.; Karim, S.; García-Etxarri, A.; Aizpurua, J. Resonant Plasmonic and Vibrational Coupling in a Tailored Nanoantenna for Infrared Detection. *Phys. Rev. Lett.* **2008**, *101*, 157403. [[CrossRef](#)] [[PubMed](#)]
5. Miroshnichenko, A.E.; Flach, S.; Kivshar, Y.S. Fano resonances in nanoscale structures. *Rev. Mod. Phys.* **2010**, *82*, 2257–2298. [[CrossRef](#)]
6. Lu, W.-T.; Wang, S.-J.; Li, W.; Wang, Y.-L.; Ye, C.-Z.; Jiang, H. Fano-type resonance through a time-periodic potential in graphene. *J. Appl. Phys.* **2012**, *111*, 103717. [[CrossRef](#)]
7. Cheng, F.; Yang, X.; Gao, J. Ultrasensitive detection and characterization of molecules with infrared plasmonic metamaterials. *Sci. Rep.* **2015**, *5*, 14327. [[CrossRef](#)] [[PubMed](#)]
8. Ma, W.; Xu, L.; Wang, L.; Kuang, H.; Xu, C. Orientational nanoparticle assemblies and biosensors. *Biosens. Bioelectron.* **2016**, *79*, 220–236. [[CrossRef](#)]
9. Chang, Y.-T.; Lai, Y.-C.; Li, C.-T.; Chen, C.-K.; Yen, T.-J. A multi-functional plasmonic biosensor. *Opt. Express* **2010**, *18*, 9561–9569. [[CrossRef](#)] [[PubMed](#)]
10. Tang, S.; Fang, Y.; Liu, Z.; Zhou, L.; Mei, Y. Tubular optical microcavities of indefinite medium for sensitive liquid refractometers. *Lab Chip* **2015**, *16*, 182–187. [[CrossRef](#)]
11. Sugawa, K.; Tahara, H.; Yamashita, A.; Otsuki, J.; Sagara, T.; Harumoto, T.; Yanagida, S. Refractive Index Susceptibility of the Plasmonic Palladium Nanoparticle: Potential as the Third Plasmonic Sensing Material. *ACS Nano* **2015**, *9*, 1895–1904. [[CrossRef](#)]
12. Lai, Y.-C.; Lee, H.-C.; Kuo, S.-W.; Chen, C.-K.; Wu, H.-T.; Lee, O.K.; Yen, T.-J. Label-Free, Coupler-Free, Scalable and Intracellular Bio-imaging by Multimode Plasmonic Resonances in Split-Ring Resonators. *Adv. Mater.* **2012**, *24*, OP148–OP152. [[CrossRef](#)]
13. Li, C.-T.; Lo, K.-C.; Chang, H.-Y.; Wu, H.-T.; Ho, J.H.; Yen, T.-J. Ag/Au bi-metallic film based color surface plasmon resonance biosensor with enhanced sensitivity, color contrast and great linearity. *Biosens. Bioelectron.* **2012**, *36*, 192–198. [[CrossRef](#)]
14. Lee, Y.; Kim, S.-J.; Park, H.; Lee, B. Metamaterials and Metasurfaces for Sensor Applications. *Sensors* **2017**, *17*, 1726. [[CrossRef](#)]
15. Abdulkarim, Y.I.; Deng, L.; Karaaslan, M.; Dalgac, S.; Mahmud, R.H.; Alkurt, F.O.; Muhammadsharif, F.F.; Awl, H.N.; Huang, S.; Luo, H. The Detection of Chemical Materials with a Metamaterial-Based Sensor Incorporating Oval Wing Resonators. *Electronics* **2020**, *9*, 825. [[CrossRef](#)]

16. Zulfi, A.; Rezeki, Y.A.; Edikresnha, D.; Munir, M.M.; Khairurrijal, K. Synthesis of Fibers and Particles from Polyvinyl Chloride (PVC) Waste Using Electrospinning. *IOP Conf. Ser. Mater. Sci. Eng.* **2018**, *367*, 012014. [[CrossRef](#)]
17. Narita, S.; Ichinohe, S.; Enomoto, S. Infrared spectrum of polyvinyl chloride. I. *J. Polym. Sci.* **1959**, *37*, 273–280. [[CrossRef](#)]
18. Chen, C.-Y.; Un, I.-W.; Tai, N.-H.; Yen, T.-J. Asymmetric Coupling between Subradiant and Superradiant Plasmonic Resonances and Its Enhanced Sensing Performance. *Opt. Express* **2009**, *17*, 15372–15380. [[CrossRef](#)]
19. Guo, L.; Chen, L.; Hong, S.; Kim, D.-H. Single plasmonic nanoparticles for ultrasensitive DNA sensing: From invisible to visible. *Biosens. Bioelectron.* **2016**, *79*, 266–272. [[CrossRef](#)]
20. Park, S.J.; Hong, J.T.; Choi, S.J.; Kim, H.S.; Park, W.K.; Han, S.T.; Park, J.Y.; Lee, S.; Kim, D.S.; Ahn, Y.H. Detection of microorganisms using terahertz metamaterials. *Sci. Rep.* **2014**, *4*, 4988. [[CrossRef](#)] [[PubMed](#)]
21. Nasir, M.E.; Dickson, W.; Wurtz, G.A.; Wardley, W.; Zayats, A.V. Hydrogen Detected by the Naked Eye: Optical Hydrogen Gas Sensors Based on Core/Shell Plasmonic Nanorod Metamaterials. *Adv. Mater.* **2014**, *26*, 3532–3537. [[CrossRef](#)]
22. Chen, X.; Fan, W. Ultrasensitive terahertz metamaterial sensor based on spoof surface plasmon. *Sci. Rep.* **2017**, *7*, 1–8. [[CrossRef](#)]
23. Wakatsuchi, H.; Greedy, S.; Christopoulos, C.; Paul, J. Customised broadband metamaterial absorbers for arbitrary polarisation. *Opt. Express* **2010**, *18*, 22187–22198. [[CrossRef](#)]
24. Fu, J.; Dong, H.; He, J.; Sun, Y.; Jin, Y.; He, S. Enabling Ultrathin Metamaterial Absorbers with Narrow Slits. *Adv. Opt. Mater.* **2020**, *8*. [[CrossRef](#)]
25. Landy, N.I.; Sajuyigbe, S.; Mock, J.J.; Smith, D.R.; Padilla, W.J. Perfect Metamaterial Absorber. *Phys. Rev. Lett.* **2008**, *100*, 207402. [[CrossRef](#)]
26. Huang, T.-Y.; Tseng, C.-W.; Yeh, T.-T.; Yeh, T.-T.; Luo, C.-W.; Akalin, T.; Yen, T.-J. Experimental realization of ultrathin, double-sided metamaterial perfect absorber at terahertz gap through stochastic design process. *Sci. Rep.* **2015**, *5*, 18605. [[CrossRef](#)]
27. Su, D.-S.; Tsai, D.P.; Yen, T.-J.; Tanaka, T. Ultrasensitive and Selective Gas Sensor Based on a Channel Plasmonic Structure with an Enormous Hot Spot Region. *ACS Sens.* **2019**, *4*, 2900–2907. [[CrossRef](#)] [[PubMed](#)]
28. Le, T.H.; Tanaka, T. Plasmonics–Nanofluidics Hybrid Metamaterial: An Ultrasensitive Platform for Infrared Absorption Spectroscopy and Quantitative Measurement of Molecules. *ACS Nano* **2017**, *11*, 9780–9788. [[CrossRef](#)] [[PubMed](#)]
29. Pryce, I.M.; Kelaita, Y.A.; Aydin, K.; Atwater, H.A. Compliant Metamaterials for Resonantly Enhanced Infrared Absorption Spectroscopy and Refractive Index Sensing. *ACS Nano* **2011**, *5*, 8167–8174. [[CrossRef](#)]
30. Pedroso, C.B.; Santos, M.B. The Lorentz model applied to composite materials. *J. Phys. Condens. Matter.* **1994**, *6*, 2395–2402. [[CrossRef](#)]
31. Levi, A.F.J. The Lorentz oscillator model. *Essent. Class. Mech. Dev. Phys.* **2016**. [[CrossRef](#)]
32. Limonov, M.F.; Rybin, M.; Poddubny, A.; Kivshar, Y.S. Fano resonances in photonics. *Nat. Photonics* **2017**, *11*, 543–554. [[CrossRef](#)]
33. Hu, F.-G.; Song, J.; Kamgaing, T. Modeling of multilayered media using effective medium theory. *Top. Meet. Electr. Perform. Electr. Packag. Syst.* **2010**, 225–228. [[CrossRef](#)]